Article

Using a Slit to Suppress Optical Aberrations in Laser Triangulation Sensors

Steven Pigeon [1,†,‡] (ID) *****, **Benjamin Lapointe-Pinel** [2,‡] (ID)

1   Université du Québec à Rimouski; steven_pigeon@uqar.ca
2   Université du Québec à Rimouski; benjamin.lapointe13@gmail.com
*****   Correspondence: steven_pigeon@uqar.ca
†   Current address: Université du Québec à Rimouski, Québec, Canada, G5L 3A1
‡   These authors contributed equally to this work.

Abstract: In this paper, we present a laser triangulation sensor to measure the distance between the sensor and an object without contact using a diffraction slit rather than a traditional lens. We show that by replacing the lens by a slit, we can exploit the resulting diffraction pattern to have finer, and yet simpler, image analysis yielding a better estimation for the distance to the object. To test our hypotheses, we build a precision position table, a laser triangulation sensor, and generated large data sets to test different estimation algorithms on various materials, comparing data acquisition using a traditional lens and using a slit. We show that the position estimation from using a slit is both more precise and more accurate than comparable methods using a lens.

1. Introduction

In many different applications, we are interested in measuring the distance between an object and a sensor without direct physical contact. When great distances are involved, the preferred approach is to use time-of-flight methods, in which a laser pulse is emitted and the time taken for the reflection to come back to the sensor is measured [1–4]. These time-of-flight sensors were pioneered in satellites [5], and are now often used in airborne exploration of regions covered in dense vegetation or otherwise inaccessible (for e.g. [6]). The accuracy of time-of-flight sensors is typically in the order of a few centimeters [7]. Acquiring distances with centimeter precision from time-of-flight sensors requires timing accuracies well under nanoseconds, as light travels 29.9792458 cm in one nanosecond. However, when time-of-flight is aided by other techniques, such as phase shift detection, accuracies in the order of 25 µm can be achieved [1, Table 5], but requires even more sophisticated, and therefore presumably even more expensive, hardware.

Laser triangulation sensors are commonly used when the distances considered between the sensor and the objects of interest are in the order of a few tens of centimeters or up to a few meters. Many of these sensors have accuracies in the order of micrometers [8–14]. Laser triangulation sensors are easier and less expensive to build than time-of-flight sensors, but they rely on image analysis algorithms to achieve precision rather than precision timing hardware.

In a laser triangulation sensor, a laser beam and the optical axis of a photosensitive sensor are placed at an angle, as schematized in fig. 1. In many applications, it is desirable to have the laser beam perpendicular to the sensor's casing, which leaves the optical assembly to be placed with a certain angle, chosen so that the optical axis (or loosely, the center of the field of view) corresponds to the center of the useful range of the sensor. As the laser beam reaches the object, it is reflected, and its reflection is projected against the photosensitive sensor through a lens or some other optical assembly. Here, we make the simplifying assumption that the laser beam and the optical axis lie in the same plane, and that this plane corresponds to one of the photosensitive sensor's axes, which will ensure that the reflected laser spot is seen as moving only along that axis—horizontally in our case—across the sensor. We can then estimate the angle of projection α, using the focal length f of
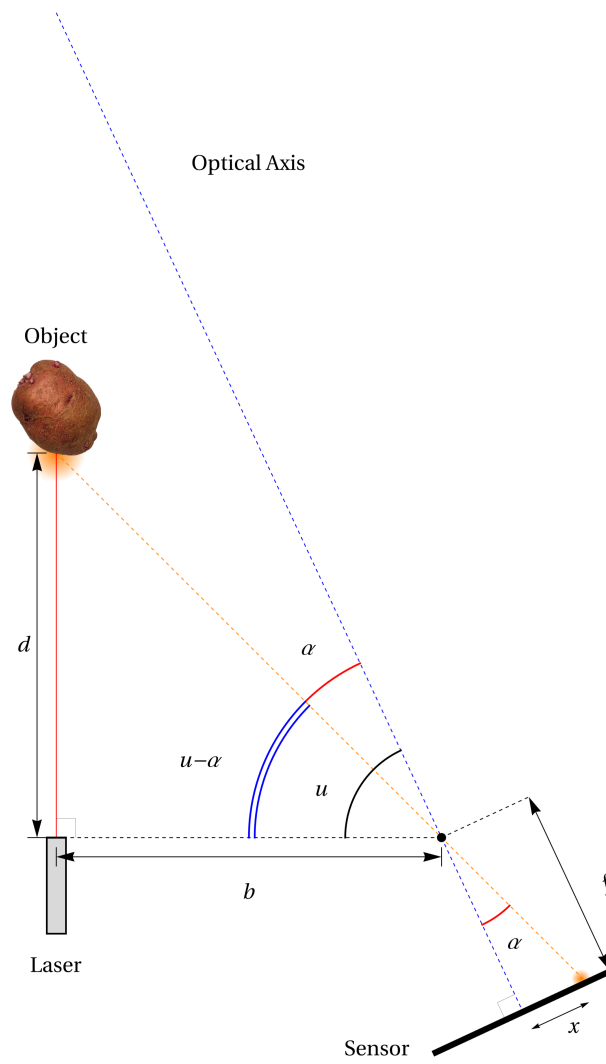
Figure 1. Laser range finding using triangulation.

the lens (or its equivalent), and the center of the projection x—the problem is therefore to obtain an accurate estimation for x, the center of the projection. Knowing the angle α, the distance b between the laser source and the center of the optical assembly, and the angle u of the assembly relative to the casing, we can determine the angle $u - \alpha$, and therefore the distance d of the target relative to the sensor.

The angle α of the projection in the optical assembly is given by

$$\alpha = \tan^{-1}\left(\frac{x}{f}\right),$$

and the distance d is found to be

$$\begin{aligned} d &= d_0 + b\tan(u - \alpha) \\ &= d_0 + b\tan\left(u - \tan^{-1}\left(\frac{x}{f}\right)\right), \end{aligned} \tag{1}$$

where d_0 is an additional offset taking into account the sensor casing thickness and other assembly variations. A first calibration procedure would be performed at the moment of assembly, and likely periodically over the sensor's lifetime in order to compensate for any mechanical changes due to temperature, vibrations, or other mishaps—none of which were tested for this proof-of-concept.
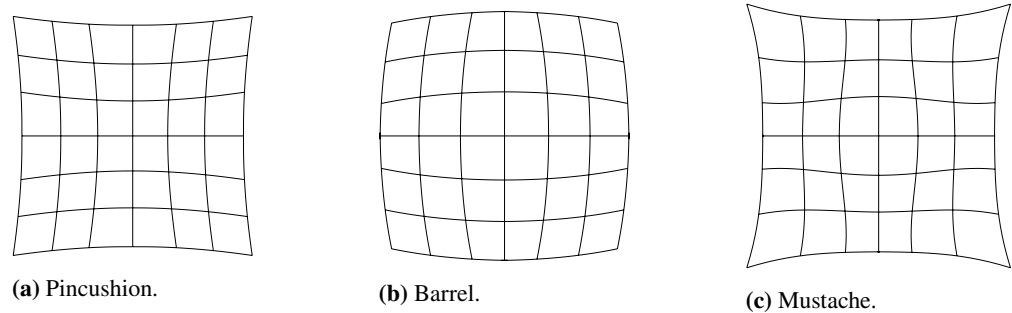
(a) Pincushion. **(b)** Barrel. **(c)** Mustache.

Figure 2. Typical optical distortions.

The preferred embodiment for the optical sensor in a laser triangulation system consists in a lens that focuses the image of the reflected laser onto a light-sensitive sensor, typically a CMOS or CCD image sensor [15–17].

However, as shown in fig. 1, the optical axis intersects the laser at an angle, which means that the focal plane of the lens, perpendicular to the optical axis, only provides a narrow region where the reflection of the laser is in good focus, as the lens will usually have a limited depth of field. To mitigate this problem, it was proposed to use so-called tilt-shift lenses to rotate the image plane in order to have the laser line entirely lying in the focal plane, according to the Scheimpflug principle [11,18]. Traditional SLR and other fixed-sensors cameras require specialty tilt-shift lenses; but in a laser triangulation sensor, we are free to change the angle of the image sensor within the device, independently from the optical axis.

Even if we suppose that we are able to use a tilt-shift lens or change the angle of the sensor to have the desired image plane, we are still bound to the limitation of the lens. Indeed, lenses are subject to a number of optical aberrations. If the lens is spherical, it will show what is called spherical aberration where different regions of the lens will have different focal points, resulting in a "soft", or diffuse, focus. If the lens have different horizontal and vertical curvatures, it will suffer from astigmatism, resulting in images clearer in one direction than the other. The lens may exhibit coma aberration, where parallel rays entering the lens at an angle will have different focal points resulting in a comet-like projection of points—thus the name. The lens can also show a number of other geometric distortions such as pincushion, barrel, or a combination of both, termed "mustache", as shown in fig. 2, which warps the projected image and therefore introduces imprecision. Additionally, all lenses are subject to chromatic aberration where rays of different wavelengths are refracted with different angles, resulting in images with a rainbow effect radial to the center of projection, typically with red fringes towards the edge of image and blue fringes towards the center. However, chromatic aberration can be safely ignored since we will use a monochromatic light source, a laser.

Although not technically an aberration, lens flare, mostly internal reflection, where light bounces around off the sensor and other optical elements, will typically produce one or several localized rings or circles of light in the image, and, if sufficiently intense, can even cause diffuse internal illumination, known as glare, that will "wash out" the whole image. This problem can be limited, but not completely eliminated, using special anti-reflective coatings on the lens elements. Lens flare will prove problematic in lens-based system, as we will show later.

Lastly, we have speckle "noise" when the laser is reflected from a rough (even microscopically) surface and interferes with itself, as it will cause the light paths to the sensors to vary in length. Speckle noise results in a granular aspect of the image. If most of the other optical aberration can be corrected or mitigated, speckle noise is unavoidable with monochromatic light [19–21].

The aberrations listed above will combine to complicate the analysis of the image, and will introduce imprecision in the estimation of the true position of the laser in the image. But mitigating these effects requires greater efforts in lens manufacturing, better and more expensive glass recipes [22], apochromatic lens assemblies if one considers using more than one color [23], etc., all of which are inapplicable for inexpensive yet precise range sensors.

If lenses are subject to so many ailments, why not dispense with them? For example, Young [24–26], drawing on the works of many other such as Mach [27], shows that, if speckle is still present
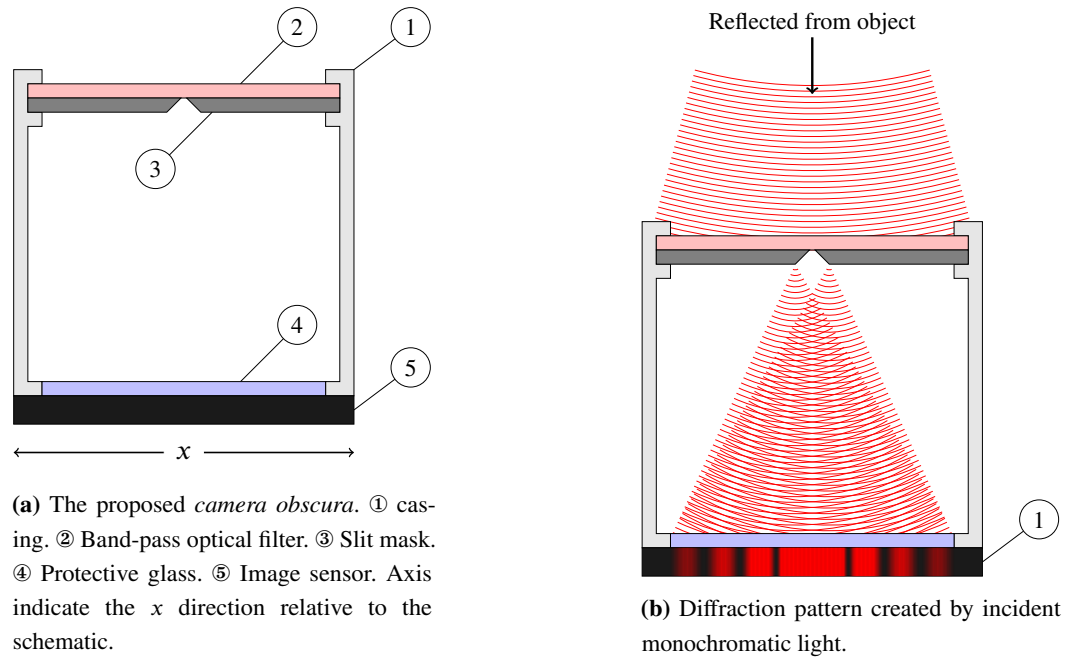
(a) The proposed *camera obscura*. ① casing. ② Band-pass optical filter. ③ Slit mask. ④ Protective glass. ⑤ Image sensor. Axis indicate the x direction relative to the schematic.

(b) Diffraction pattern created by incident monochromatic light.

Figure 3. The proposed *camera obscura*. In 3a, parts labeled. In 3b, the diffraction pattern.

(as it depends mostly on the surface from which the laser is reflected), a pinhole camera eliminates spherical, coma, and other defocussing aberrations, and that it does not introduce field curvature or other distortions in the image. He also shows that pinhole cameras have a theoretically infinite depth of field, or, at least in practice, much greater than a lens. It can also offer a much wider field of view, in principle up to 180°—it will, however, be limited by the thickness of the plate and the diameter of the hole[1]. A pinhole camera is susceptible to chromatic aberration, but in our case, we can safely ignore this problem as monochromatic light will be used. The pinhole camera is also susceptible to astigmatism if the pinhole is not perfectly circular (or if the object is at an angle relative to the optical axis, the aperture will appear as an ellipse), but if mild astigmatism is undesirable, we will show that extreme astigmatism can be favorably exploited.

Indeed, in this paper, we will show that replacing almost all the optical components by a single slit in a laser triangulation range sensor circumvents most optical aberrations, nearly eliminates lens flare, and reduces speckle, thus greatly reducing the need for software correction of aberrations. Furthermore, we will make the case that such a sensor is much simpler and is less expensive to manufacture than conventional lens-based sensors, as well as potentially more accurate.

2. Hypotheses

Since a pinhole camera avoids most optical aberrations, offers potentially both a very wide field of view and an infinite depth of field (or at least, vastly larger than a conventional lens), reduces lens flare and other internal reflections, we suppose it can be used for a laser triangulation sensor and that we can exploit the diffraction patterns to have better algorithms and better estimation of the laser spot position.

The proposed camera configuration is shown in the simplified diagram of fig. 3. The triangulation sensor is composed of only four elements. We find an outer casing, shown as ① in the figure, that holds the band-pass filter, ②, the slit mask, ③, and the image sensor, shown with its protective window ④ and package ⑤. The actual setup, that will be discussed in the next section, built from readily available hardware, differs very little in its principles.

The band-pass optical filter will block all light except for a narrow band of wavelengths corresponding to the laser used. This allows the sensor to operate in essentially monochromatic light.

---

1   For plate thickness t and hole diameter d, the field of view will be $2\tan^{-1}(d/t)$, which will be 180° only as $t \to 0$ or $d \to \infty$, with an infinite plane for the sensor; clearly, and infeasible solution. However, pinholes and slits are often beveled on the interior side (◤▬◥) to widen the view angle.
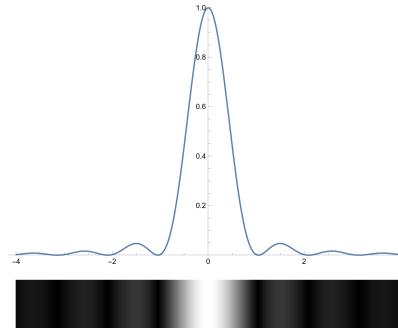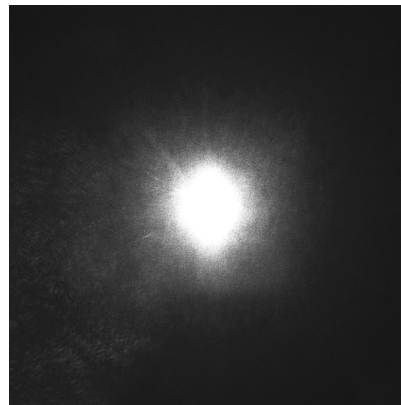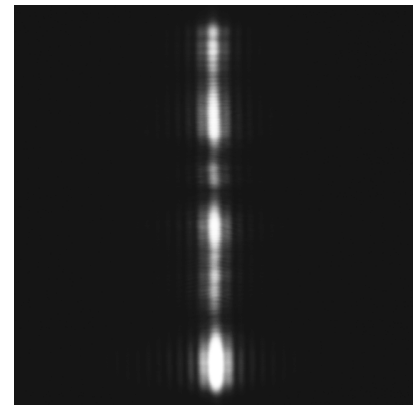
Figure 4. Fraunhofer diffraction (normalized intensity).

(a) with a lens.

(b) With a slit.

Figure 5. Projection of the laser spot with a lens in (a), and a slit in (b).

In monochromatic light, the light entering the sensor will interfere with itself and create a specific interference pattern: an Airy diffraction pattern, a disk if the aperture is circular [28] or a central bright band with progressively less intense side-bands on each side if the aperture is a slit, as shown in fig. 4 [29, § 8.5]. If the projected laser image takes a pattern of a known or expected form, then we should be able to exploit this knowledge to obtain a better fit on the image and a better estimate for the true center of the spot.

As we mentionned earlier, if pinhole cameras are not subject to as many optical aberrations as lens-based cameras, we still have to worry about speckle noise. Speckle noise originates in the surface of the object from which the laser is reflected. The object surface asperities, whether very rough or minute, will give the reflected light different path lengths to the sensor, and therefore different phases, where it will interfere with itself, giving the image a granulated aspect, as shown in fig. 5a.

To reduce the effect of speckle, we use a vertical slit (relative to the horizontal axis to the image sensor sensor) rather than a circular aperture. This can be seen as a special case of astigmatism, where in one direction (along the slit) the focal length is very large and along the other (across the slit) the focal length is short. This causes a stretch in the reflected laser image, as shown in fig. 5b. In this way, speckle noise is spread mostly vertically, allowing a better horizontal, line by line, analysis of the image. We also suppose that the projection angle (α in fig. 1) is moderate so that the projected image, the interference pattern, remains approximately symmetrical [30].

If the general shape of the projected image is known, we can use a better algorithm than a simple centroid to find its center. The models considered are the simplified gaussian function (not to be confused with the gaussian distribution) and the Fraunhofer diffraction formula, an approximation to the Airy diffraction pattern. Once a good estimate of the center of the projected image is obtained, we can translate from pixel space to actual distance. One possible way to do so is to use a geometric model that takes into account the various parameters of the sensor, and translate the projection center x to the distance d, just as shown in fig. 1. Another way would be to place the sensor on a high-precision linear displacement table and to acquire a number of laser point reflections from a target at known positions. These points are to be stored in a look-up table in the sensor, and a new position x in pixel
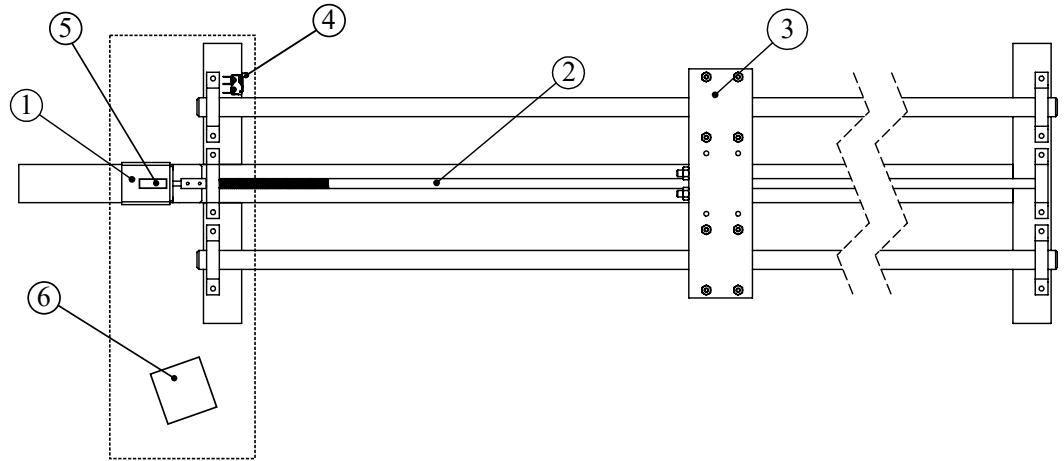
Figure 6. A simple high-precision position table. Useful range: 150 cm. ① step motor, ② worm gear, ③ target carriage, ④ limit switch. On a metal plate (dashed): ⑤ laser, ⑥ camera with lens or slit.

space can be searched in the table, and the distance d interpolated from neighboring known values in the table. This second method seems suboptimal, but it may be preferable as it takes into account any deviation from the ideal device due to manufacturing.

Therefore, our main hypothesis is that replacing a lens by a slit improves the accuracy of a laser triangulation sensor. The use of a slit circumvents most of the optical aberrations found in lenses, reduces the influence of speckle noise, and aids image analysis by creating (mostly) symmetrical diffraction patterns. Symmetrical diffraction patterns could be amenable to simpler, or less computationally expensive, image analysis algorithms. As a side-effect, we surmise it will reduce significantly the mechanical complexity and cost of manufacturing of laser triangulation sensors, as well as potentially making them more robust and easier to adjust and calibrate.

3. Methods

To create a useful data set, we built a precision position table to move with accuracy a target on which to reflect the laser and support the instruments such as the table's controller, the laser source, and the camera. The table is fully automated under the control of a standard PC and over a serial/USB cable.

The precision positioning table is shown in fig. 6. Controlled by a precision step motor capable of 6400 steps by revolution (shown as ① in the figure), a worm gear ②, and a carriage ③ on which we can place different materials. The useful range of the table is 150 cm, starting at the limit switch, shown as ④. Since during acquisition, the carriage was only moved in one direction (away from the camera), there is no kick back as the worm gear only pushed against the carriage. The displacement error, after 60 000 steps, was well under 1 mm, which gives us displacements of 25 μm ± 0.017 μm per acquisition.

The laser is a Class IIIa 650 nm 5 mW 5 V TTL red laser diode, and is placed over the step motor and in the same orientation as the worm gear, shown as ⑤ in the figure.

The camera used, shown as ⑥ in the figure, is a C-Mount Sentech STC-MBS231U3V USB3 camera. The camera has a resolution of 1920 × 1200 pixels over a 7.04 mm × 11.3 mm CMOS full-shutter image sensor. The camera uses a Sony IMX249 monochrome image sensor, which produces a gray-tone image and therefore avoids any artifacts that would result from a Bayer color filter sensor. The maximum frame rate for the camera at full resolution is 41.6 fps, but the camera was used in snapshot rather than in movie mode. The camera was placed 30 cm away from the laser and angled so that its optical axis crosses the worm gear.

For the images themselves, we produced for each material two sets of images, one using a lens, another using a slit. For the image acquisition with a lens, a Computar 50mm fixed focal length, f/1.8, C-mount lens was used, with the iris set at f/12 to have an image illumination comparable to the slit. For the images acquired with a slit, we used a 25.4 mm diameter slit disk compatible with the C mount 50mm tube, with a 200 μm × 3 mm slit centered slit.

The materials used for the tests were chosen to be representative of textures likely encountered in primary or secondary sector processes or manufacturing. The material chosen were brushed metal; unevenly rusted metal; light-colored, planed but unvarnished, wood; standard white printer paper; black and reflective PVC (black electrical tape); and microfiber fabric.

The acquisition strategy was straightforward. For each configuration, we started the carriage at the beginning of the useful range of the sensor, that is, when the laser spot happens to be fully captured. This correspond to 60 cm away from the carriage pushed against the limit switch (④ in fig. 6). The slit field of view is naturally wider than the lens', but both begin at 60 cm from the limit switch. We then proceeded to acquire 5 independent 1920×600 images (with the region of interest centered vertically in the 1920×1200 complete image), then moved the carriage forward to the right, relative to fig. 6 by 25 µm. The process was repeated until it reached the end of sensor range, (where the spot stops being visible), 102 cm away from the limit switch, which amounts to 16800×5 captures. This process was done for each pair of material and lens or slit combination.

After all lens, slit, and other aberrations, the image sensor itself is noisy. For the CMOS image sensor, there are two type of noise. The first one is thermal noise that will make each pixel value change randomly. It is usually supposed to be small and independent and identically normally distributed. The second type of noise is the black threshold where pixels report values much higher than zero despite not being exposed. We will consider this black threshold as a shared systematic bias: while individual pixels might be "hotter" than others, we will suppose they all have the same bias.

This bias should therefore be removed before proceeding to further image analysis to find the center of the reflected laser spot. The black threshold, t, can be estimated once at calibration or it can be estimated for each image. To estimate the black threshold for an image, we average all pixels of the image except for the region containing the reflected laser spot. The reflected laser spot position is first estimated coarsely using the centroid, or center of mass of the image. That is, for a $n \times m$ pixel image, the centroid is given by

$$c = \frac{\sum_{i=1}^{n} \sum_{j=1}^{m} y_{i,j}(i,j)}{\sum_{i=1}^{n} \sum_{j=1}^{m} y_{i,j}}, \tag{2}$$

where $y_{i,j}$ is the intensity of the pixel at coordinates (i,j), understood as a two-dimensional vector. The centroid is then used as the center of a 320×600 pixels exclusion region for the lens and a 128×600 pixels exclusion region for the slit.

Once t is estimated, we correct the pixel values to compensate for the black threshold without renormalization, that is,

$$y'_{i,j} = \max(0, y_{i,j} - t).$$

We are now ready to find the center of the reflected laser spot. We will have two distinct cases to consider, one where the spot is projected by a lens and is approximately circular, as shown in fig. 5a; another where the spot is projected through the slit, as shown in fig. 5b.

Ross describes some typical ways of finding the center of a reflected laser spot projected by a lens [31]. We chose a simplified gaussian function,

$$A_{max} \, e^{-\|r\|^2}, \tag{3}$$

where A_{max} is the maximum amplitude at the center, and r is a linear transformation applied to the coordinates of the image plane,

$$r = \begin{bmatrix} \sigma_{xx} & \sigma_{xy} \\ \sigma_{yx} & \sigma_{yy} \end{bmatrix}^{-1} \begin{bmatrix} x - \mu_x \\ y - \mu_y \end{bmatrix}. \tag{4}$$

The amplitude A_{max}, the covariances $\sigma_{xx}, \sigma_{xy}, \sigma_{yx}, \sigma_{yy}$, the means μ_x and μ_y will be estimated using least mean squares regression. The values for μ_x and μ_y will give us the center of the reflected laser spot.
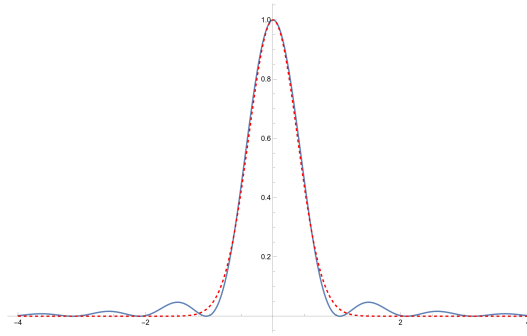
Figure 7. Fraunhofer diffraction (blue) approximated as a gaussian (dashed red).

For the images captured using the slit, we will proceed to a line by line analysis, fitting a one-dimensional gaussian function,

$$A_{max}\, e^{-\left(s(x-x_0)\right)^2}. \tag{5}$$

where x_0 is the center, s contains the wave-number and other scalings, and A_{max} is the maximum amplitude. This approximation is quite reasonable, as shown in fig. 7. The side lobes in the Fraunhofer diffraction formula, eq. (6), vanish rapidly and the gaussian function, eq. (3) (or eq. (5)), very closely matches the central peak.

We see from fig. 7 that a simplified gaussian is a good approximation to the actual Fraunhofer diffraction formula given by

$$F(x) = A_{max}\, \text{sinc}^2\left(s\left(x - x_0\right)\right). \tag{6}$$

The Fraunhofer formula, however, should be much closer to the actual projection being observed and, once fitted, is potentially a much better estimate of the actual center of the reflected laser spot, but using the simplified gaussian of eq. (5) will be less computationally intensive for the sensor's onboard processor.

The final slit center will be estimated as the average of all line by line centers, either estimated by the simplified gaussian or by the Fraunhofer diffraction formula. These averagings yield good estimates of the horizontal position of the reflected laser spot. Indeed, for the images captured using the slit, the projections only move horizontally as the laser and the optical axis are in a same plane parallel to the x-direction of the image sensor.

Once x is estimated by either the centroid, the simplified 2D gaussian for images captured with a lens, or by the line-by-line average using simplified gaussian or Fraunhofer's formula for images captured with the slit, we use eq. (1) to estimate the distance to the sensor. However, eq. (1) contains a number of parameters that must be found. For example, to use eq. (1) using a slit and Fraunhofer's formula, we use all the images from a data set captured using a slit and estimate all the xs using Fraunhofer's formula, then use these xs and their corresponding known positions to fit the parameters of eq. (1) using a modified least mean squares approach [32]. The errors reported in section 4 are the differences between the positions predicted from eq. (1) and the known positions.

4. Results

In this section, we will present the results from the experimental setup described in the previous section. We will show that the positions estimated by the fit of the simplified gaussian function on the reflected laser spot projected by a lens are not as precise as the positions estimated by both the fit of the simplified gaussian function and by the fit of the Fraunhofer diffraction formula over the reflected laser spot captured using a slit.

First, let us discuss the translation from an estimation of the center x to the distance d, as given by eq. (1). If d_0, u, b, and f are known with high certainty, the translation is done quite easily. If they are not, or not known with great precision, we can use the data and fit eq. (1) on the data to find the parameters $\hat{d}_0$, $\hat{u}$, $\hat{b}$, and $\hat{f}$ that best fit the observations. Fig. 12a, for example, shows such a fit for the positions obtained from a sensor using a slit. This will allow us to assess the quality of the estimates on the positions of the reflected laser spot, whether through a lens or a slit.
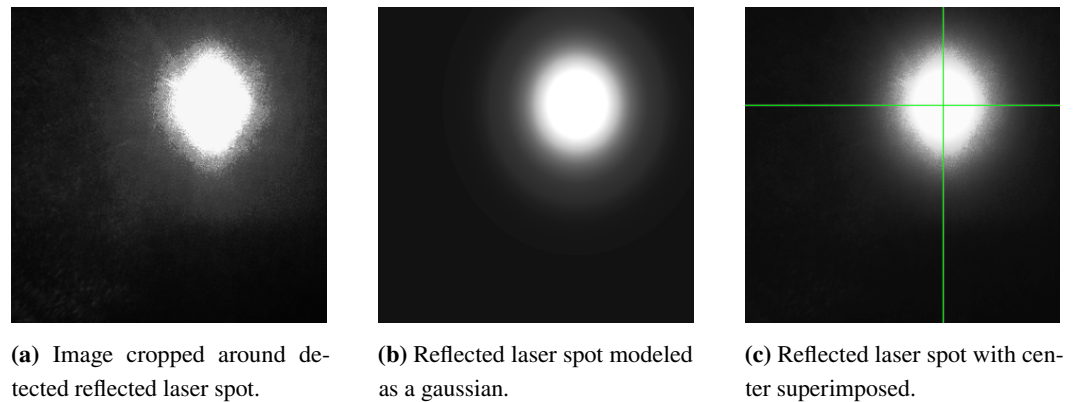
(a) Image cropped around detected reflected laser spot.

(b) Reflected laser spot modeled as a gaussian.

(c) Reflected laser spot with center superimposed.

Figure 8. Analysis of a laser spot through a lens.

(a) Image cropped around detected reflected laser spot.

(b) Reflected laser spot with centers, line-by-line.

(c) Reflected laser spot with center superimposed.
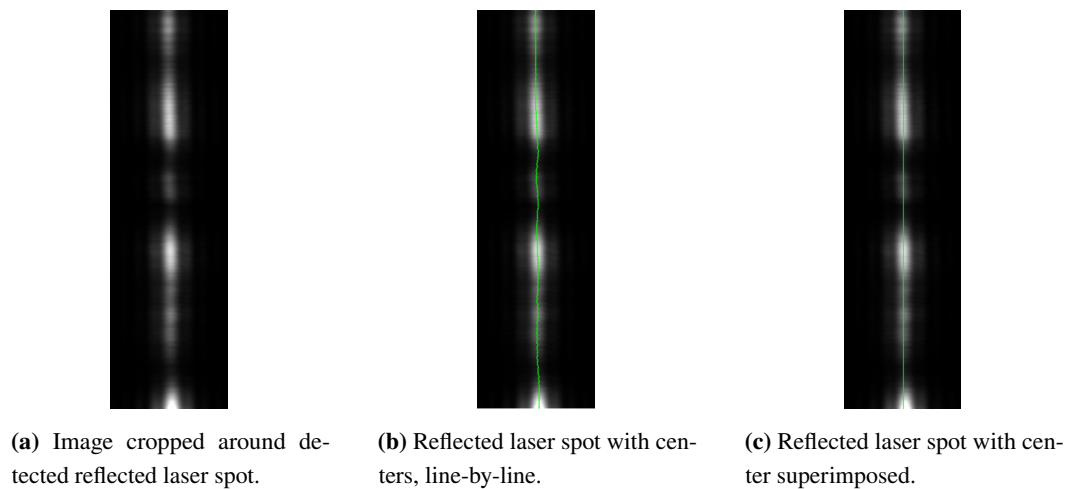
Figure 9. Reflected laser spot through a slit.

Let us now present the results obtained from a sensor using a lens. First, we examine its behavior and properties. In fig. 8a, we observe the cropped reflected laser spot through a lens. We see that it is diffuse, despite being in focus, and that it exhibit conspicuous, but as remarked earlier, unavoidable, speckle noise. We also see that the spot is not perfectly circular but elongated. This is the effect of the laser beam not being perfectly circular interacting with the target material, in this particular example, white printer paper. In fig. 8b, we see the best-fit gaussian obtained from the raw data. From this fit parameters, we obtain the estimation for the center of the spot, shown in fig. 8c as a green cross.

In fig. 10a, we see the errors in mm between the estimated positions using a lens and the true position. The position of the reflected laser spot is estimated for each measurement. It is then translated into actual distance using eq. (1) with its parameters estimated on the whole data set. We see that the predicted distances are precise but not very accurate. At both far left and far right, the readings are thrown off by optical aberrations. The variation near the center is caused by lens flares, more visible as the laser spot approaches the center of the image.

The process is quite similar when using a slit. In fig. 9a, we see the cropped image of the isolated reflected laser spot. For each line, a gaussian is fitted, as is shown in fig. 11, and the center is estimated for that line. We see all the line-by-line centers found in fig. 9b. These centers are averaged to obtain the final estimate of x, the horizontal position of the spot, as projected through the slit. The process is similar (but not shown in the figures) for the fit using Fraunhofer's diffraction formula.

Fig. 12a shows the result of the estimation of the different parameters of eq. (1) fitted on all the centers found using all the centers estimated using the slit for white printer paper data set. Fig. 12a show that if the curve does not go through every point—as it could not, since eq. (1) is rather constrained—but that, on average, the errors are very small. Fig. 12b shows the discrepancy between known positions (obtained during the target displacement by the precision position table) and the prediction from eq. (1) with its parameters estimated from the computed centers. Lastly, fig. 10b
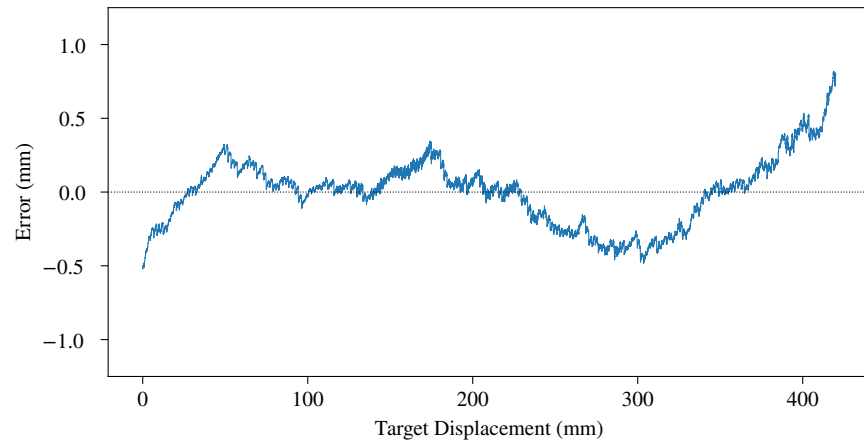
(a) Errors on center estimation from using a lens.
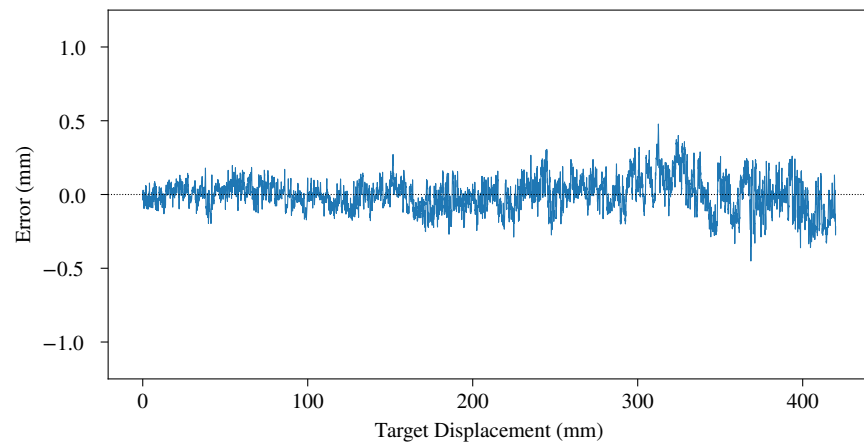
(b) Errors on center estimation from using a slit.

Figure 10. Errors on center estimations from both methods. The material measured in this figure is the brushed metal.
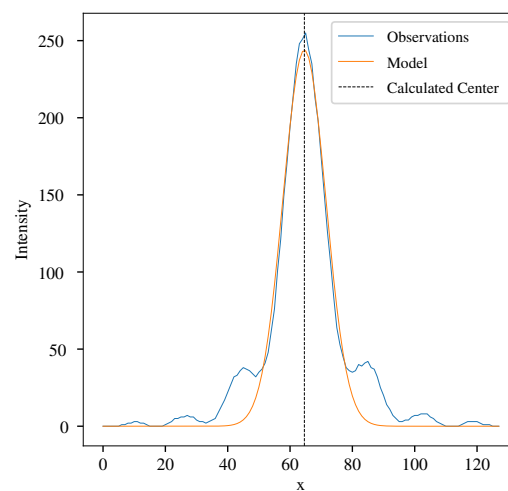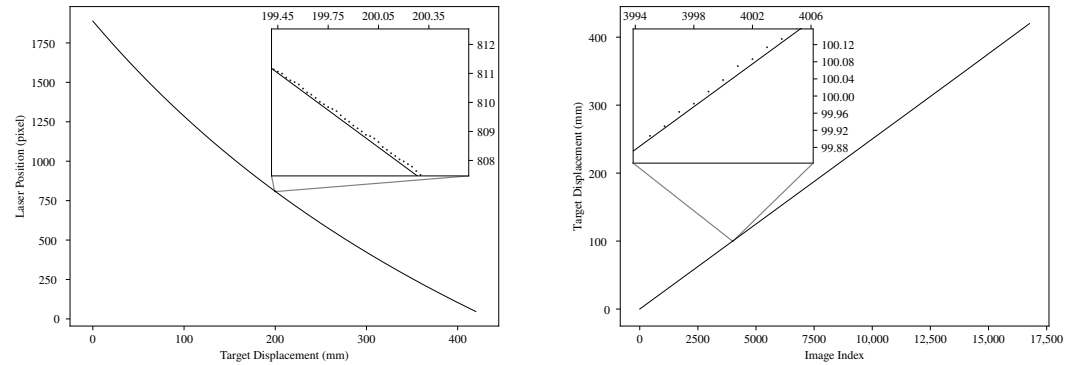

Figure 11. Gaussian fitted to a single line observation.

(a) Geometric model fitted on slit data. Dots are estimated centers from image analysis, straight line is eq. (1) fitted on the data.

(b) Known positions *vs* fitted geometric model. The dots are known (discrete) positions, the line is the prediction from the geometric model.

Figure 12. Geometric model, fit, and positions.

	Lens		**Slit With Gaussian Fit**		**Slit With Fraunhofer Fit**	
Material	**MAX**	**MAE**	**MAX**	**MAE**	**MAX**	**MAE**
	µm	µm	µm	µm	µm	µm
Brushed Metal	851	182	520	115	527	155
Rusty Metal	860	164	640	158	638	158
Light Wood Plank	651	151	429	72	476	81
Printer Paper	812	144	468	81	437	72
Black Electric Tape	1098	280	735	134	743	134
Microfiber Fabric	677	154	602	118	600	119

Table 1. Compared measurement errors for different materials.

shows that the slit is more accurate *and* more precise than the lens. It shows that the sensor using a slit is not affected by flares, and so, in average, is closer to the real value than the sensor using the lens.

Table 1 compares the maximum error (MAX) and the mean average error (MAE) for the lens, the slit with a gaussian fit, and the slit using Fraunhofer's diffraction formula, given the material chosen. In all cases, the slit methods are better than the lens, and sometimes significantly so. This also corroborates our interpretation that using a slit leads to results that are both more precise and more accurate than using a lens. This interpretation of the results is also confirmed by the violin plots of fig. 13. Violin plots are an extension of plots where probability densities are superposed to quartiles. From fig. 13, it is apparent that the distributions of errors from the slit (in tan ■ for the gaussian function and in rose ■ the Fraunhofer diffraction formula) are all more compact than the distributions of errors from the lens (in slate ■). We also remark that the error distributions from the lens are multi-modal, while this effect is much less present with the slit methods, as the optical aberrations, being almost eliminated, do not perturb the estimation as much.

5. Discussion

The results seem to indicate that using a slit in a laser triangulation sensor is a promising avenue. Indeed, fig. 10 shows that a laser triangulation sensor using a slit is less subject to various optical aberrations, in particular lens flare. The results also show that on average, the sensor using a slit is both more precise and more accurate than the sensor using a lens.

However, the proposed method is not without flaws. First, it depends on the wavelength of the laser. In our experiments, we chose a Class IIIa 650 nm red laser both out of convenience (as it is readily available) and safety (as it is mostly harmless), but a shorter wavelength laser could be
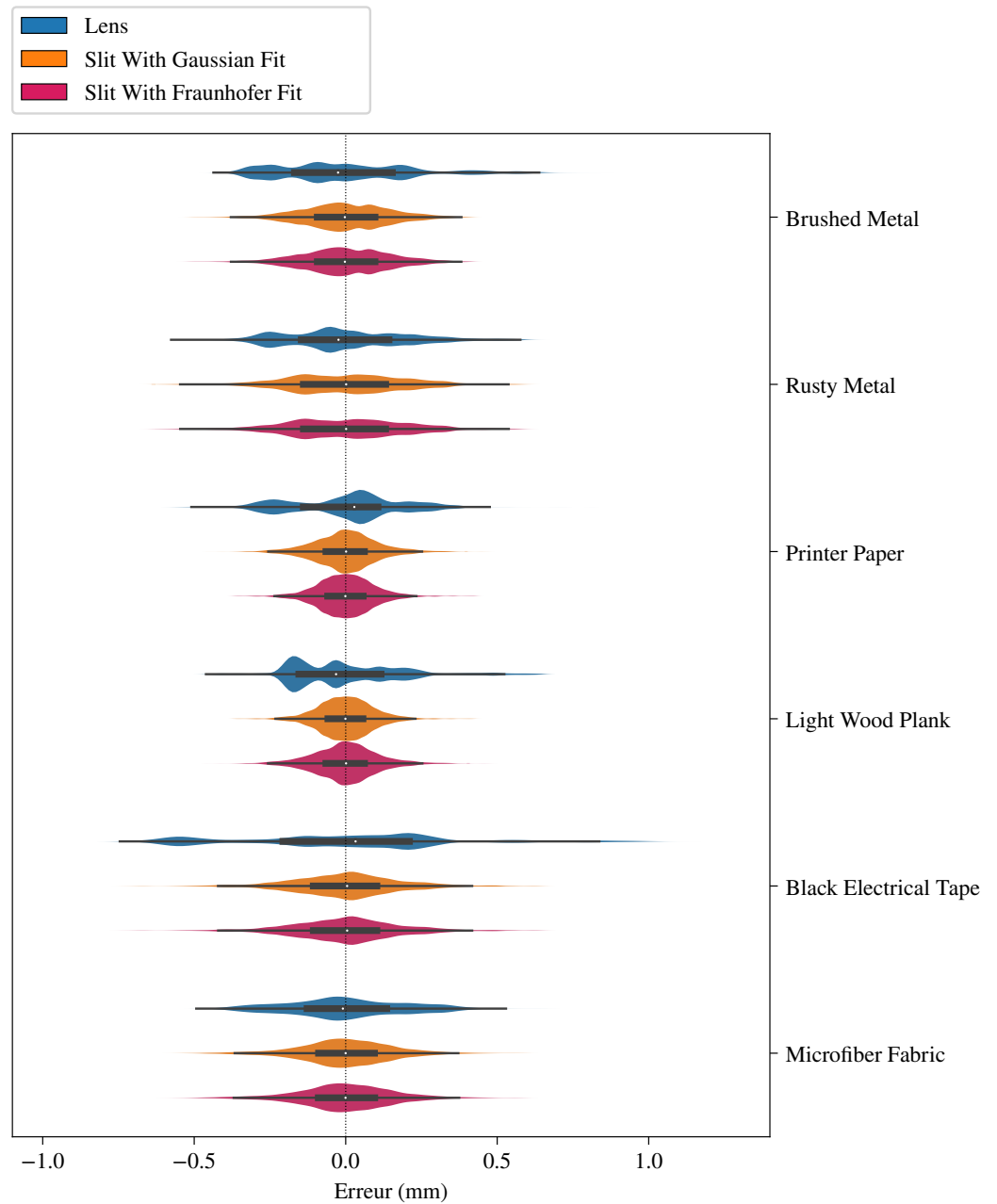
Figure 13. Violin plots of errors for lens compared to slit. The *x*-axis shows the magnitude of errors (dashed line is zero), the *y*-axis is normalized probability.

used. The spread of the diffraction pattern is strongly linked to the incident wavelength; a shorter wavelength would yield both a more compact diffraction pattern and finer-grained speckle which, if fine enough, could be averaged within pixels by the CMOS sensor itself. Second, we could use a more powerful laser, which would counteract the relative "darkness" of a camera using a slit aperture. For the tests, we had the luxury of higher exposure times to gather enough light to form images clear enough for analysis, but some applications might necessitate a great number of readings per second, and therefore, very short exposure times. Additionally, if greater distances are considered, wavelength and power can be chosen to accommodate the specific application considered [33]. Thirdly, using simplified functions (such as the simplified gaussian or the Fraunhofer diffraction formula) certainly deprives us of a better fit we might obtain from a formula such as the Fresnel diffraction formula. Indeed, better exploiting information in the diffraction pattern could not only give us a better estimation for the position of the maximum, but also give us information about the angle of incidence, as the diffraction pattern is approximately symmetric only for small angles. Better estimation algorithms will be the subject of future work. Lastly, precision is affected by the materials measured. Rough, porous, or irregular specular reflection materials will prove difficult to measure accurately—regardless of the laser spot acquisition method.

The simplified hardware required is also quite interesting. In both systems—lens and slit—we find a band-pass optical filter, that conveniently filters out undesired light sources, and an image sensor—typically CMOS. But a slit, even precision-manufactured, is much less expensive, and resource-consuming than a lens, especially that "a lens" is rarely just one piece of glass, more often a rather complicated assembly comprising many lenses, designed to compensate for all kinds of optical aberrations [34,35]. Furthermore, as we showed that the reflected laser spots only travels horizontally in the field of view, we might not need a full sensor and a line-scan sensors (which, despite the name, typically includes more than one rows of pixels) could suffice. Such an image sensor would also reduce the cost and size of the laser triangulation sensor.

The image analysis algorithms are also likely to be simpler when we explicitly exploit the shape of the diffraction pattern. In the case of a full two-dimensional gaussian, we either must explicitly and directly estimate the covariance matrix Σ and compute its inverse (as in eq. (4)) using the usual estimation method, $\Sigma = \frac{1}{n}(XWX^T - n\vec{\mu}\vec{\mu}^T)$, with W being the weights (pixel intensities), X the column-vector matrix of pixel coordinates, and $\vec{\mu}$ the average coordinate—the centroid—or we use some other regression framework, as, for example, L-BFGS-B that was used for our experiments [36–39]. For a one-dimensional fit, the estimation of center and spread is much simpler and each line could be, at least in principle, processed in parallel.

We are now confident that the method can be exploited for laser triangulation sensors.

6. Conclusions

The starting hypotheses was that using a slit instead of traditional lenses in a laser triangulation sensor could improve the accuracy of the sensors by removing the optical aberrations inherent to lenses and that a slit could be amenable to simpler analysis algorithms, or at least less computationally expensive. We have shown that line-by-line analysis of the diffraction pattern of a reflected laser spot through a slit is not only simpler but gives more accurate results than the image analysis of a reflected laser spot through a lens, and this, for both fit methods (simplified gaussian and Fraunhofer's diffraction formula) for all considered test materials.

Further work is of course considered. Preliminary testing seems to indicate that the gain from using the Fraunhofer diffraction formula to find the center is negligible compared to the simple gaussian approximation, but we intended to explore more complex models of the diffraction pattern, especially to take the asymmetry arising from larger incident angles into account.

References

1. Blais, F. Review of 20 years of range sensor development. *Journal of Electronic Imaging* **2004**, *13*, 231. https://doi.org/10.1117/1.1631921.
2. Antonio, M. Three dimensional camera and range finder. 5081530A, 1992.
3. Hsu, S.; Acharya, S.; Rafii, A.; New, R. Performance of a Time-of-Flight Range Camera for Intelligent Vehicle Safety Applications. In *Advanced Microsystems for Automotive Applications 2006*; Valldorf, J.; Gessner, W., Eds.; Springer: Berlin, Heidelberg, 2006; pp. 205–219. https://doi.org/10.1007/3-540-33410-6-16.
4. Gokturk, S.; Yalcin, H.; Bamji, C. A Time-Of-Flight Depth Sensor—System Description, Issues and Solutions. In Proceedings of the 2004 Conference on Computer Vision and Pattern Recognition Workshop. IEEE, 2004, p. 35. https://doi.org/10.1109/cvpr.2004.291.
5. Fouladinejad, F.; Matkan, A.; Hajeb, M.; Brakhasi, F. History and Applications of Space-Borne LIDARs. In Proceedings of the The International Archives of the Photogrammetry, Remote Sensing, and Spatial Information Sciences, 2019, Vol. XLII-4W18, pp. 407–414.
6. Šprajc, I.; Inomata, T.; Aveny, A.F. Origins of Mesoamerican astronomy and calendar: Evidence from the Olmec and Maya Regions. *Science Advances* **2023**, *9*. https://doi.org/https://doi.org/10.1126/sciadv.abq7675.
7. Specification for Airborne LiDAR for the Province of British Columbia, Version 5.3. Technical report, GeoBC/Ministry of Water, Land and Resource Stewardship, 2023.
8. Bosch, T. Laser ranging: a critical review of usual techniques for distance measurement. *Optical Engineering* **2001**, *40*, 10–19. https://doi.org/10.1117/1.1330700.
9. Barreto, S.V.F.; Sant'Anna, R.E.; Feitosa, M.A.F. A method for image processing and distance measuring based on laser distance triangulation. In Proceedings of the IEEE 20th International Conference on Electronics, Circuits, and Systems (ICECS), 2013, pp. 695–698. https://doi.org/10.1109/ICECS.2013.6815509.
10. Clarke, T.A.; Grattan, K.T.V.; Lindsey, N.E. Laser-based triangulation techniques in optical inspection of industrial structures. In Proceedings of the Optical Testing and Metrology III: Recent Advances in Industrial Optical Inspection; Grover, C.P., Ed. SPIE, 1991, Vol. 1332, pp. 474–486. https://doi.org/10.1117/12.51096.
11. Donges, A.; Noll, R. *Laser Measurement Technology*; Springer Berlin Heidelberg, 2015. https://doi.org/10.1007/978-3-662-43634-9.
12. Ji, Z.; Leu, M. Design of optical triangulation devices. *Optics & Laser Technology* **1989**, *21*, 339–341. https://doi.org/10.1016/0030-3992(89)90068-6.
13. Kumar, S.; Tiwari, P.K.; Chaudhury, S. An optical triangulation method for non-contact profile measurement. In Proceedings of the 2006 IEEE International Conference on Industrial Technology. IEEE, 2006, pp. 2878–2883. https://doi.org/10.1109/icit.2006.372653.
14. Swojak, N.; Wieczorowski, M.; Jakubowicz, M. Assessment of selected metrological properties of laser triangulation sensors. *Measurement* **2021**, *176*. https://doi.org/10.1016/j.measurement.2021.109190.
15. Fossum, E.R. Active Pixel Sensors: Are CCDs Dinosaurs? In Proceedings of the Procs. Charged Compled Devices and Solid-State Optical Sensors III, 1993, pp. 2–14. (SPIE vol. 1900).
16. Fossum, E.R.; Hondongwa, D.B. A Review of the Pinned Photodiode for CCD and CMOS Image Sensors. *IEEE Journal of the Electron Devices Society* **2014**, *2*, 33–43.
17. Renshaw, D.; Denyer, P.B.; Wang, G.; Lu, M. ASIC Image Sensors. In Proceedings of the Procs. IEEE Int. Symposium on Circuits and Systems, 1990, pp. 3038–3041.
18. Scheimpflug, T. Improved Method and Apparatus for the Systematic Alteration or Distortion of Plane Pictures and Images by Means of Lenses and Mirrors for Photography and for other purposes. 190401196A, 1904.
19. Baribeau, R.; Rioux, M. Influence of speckle on laser range finders. *Applied Optics* **1991**, *30*, 2873–2878. https://doi.org/10.1364/ao.30.002873.
20. Baribeau, R.; Rioux, M. Centroid fluctuations of speckled targets. *Applied Optics* **1991**, *30*, 3752–3755. https://doi.org/10.1364/ao.30.003752.
21. Dorsch, R.G.; Häusler, G.; Herrmann, J.M. Laser triangulation: fundamental uncertainty in distance measurement. *Applied Optics* **1994**, *33*, 1306–1314. https://doi.org/10.1364/AO.33.001306.
22. Zhang, A.; Youngworth, R.N., Eds. *Review of Optical Manufacturing 2000 to 2020*; SPIE Press, 2021.
23. Gruescu, C.; Nicoara, I.; Popov, D.; Bodea, R.; Hora, H. Optical Glass Compatibility for the Desing of Apochromatic Systems. *Science of Sintering* **2008**, *40*.
24. Young, M. Pinhole Optics. *Applied Optics* **1971**, *10*, 2763–2767. https://doi.org/10.1364/ao.10.002763.
25. Young, M. Pinhole Imagery. *American Journal of Physics* **1972**, *40*, 715–720. https://doi.org/10.1119/1.1986624.
26. Young, M. The Pinhole Camera: Imaging without Lenses or Mirrors. *The Physics Teacher* **1989**, *27*, 648–655.
27. Mach, E. *Die Prinzipien der physikalischen Optik: Historisch und erkenntnispsychologisch entwickelt*; Verlag von Johan Ambrosius Barth, 1921.

28. Airy, S.G.B. *On the Diffraction of an Object-glass with Circular Aperture*; Vol. V, Printed at the Pitt Press by John Smith, 1835; pp. 283–291.

29. Born, M.; Wolf, E.; Bhatia, A.B.; Clemmow, P.C.; Gabor, D.; Stokes, A.R.; Taylor, A.M.; Wayman, P.A.; Wilcock, W.L. *Principles of Optics*; Cambridge University Press, 1999. https://doi.org/10.1017/cbo9781139644181.

30. Biswas, S.; bhattacharyya, R.; Bhattacharyya, S. Explicit Derivation of the Fraunhofer Diffraction Formula for Oblique Incidience. *European Journal of Physics* **2021**, *43*, 015301:1–015301:5.

31. Ross, T.S. *Laser Beam Quality Metrics*; SPIE: Bellingham, Washington 1000 20th St. Bellingham WA 98225-6705 USA, 2013.

32. Sorensen, D.C. Newton's Method with a Model Trust Region Modification. *SIAM J. on Numerical Analysis* **1982**, *19*, 409–426.

33. Fahey, T.; Islam, M.; Gardi, A.; Sabatini, R. Laser Beam Atmospheric Propagation Modelling for Aerospoce LIDAR Applications. *Atmosphere* **2021**, *12*, 918:1–918:47.

34. Cox, A. *A System of Optical Design*; Focal Press, 1964.

35. Cox, A. *Photographic Optics*, 15th ed.; Focal Press, 1974.

36. Broyden, C.G. The Convergence of a Class of Double-rank Minimization Algorithms 1. General Considerations. *IMA Journal of Applied Mathematics* **1970**, *6*, 76–90. https://doi.org/10.1093/imamat/6.1.76.

37. Fletcher, R. A new approach to variable metric algorithms. *The Computer Journal* **1970**, *13*, 317–322. https://doi.org/10.1093/comjnl/13.3.317.

38. Goldfarb, D. A family of variable-metric methods derived by variational means. *Mathematics of Computation* **1970**, *24*, 23–26. https://doi.org/10.1090/s0025-5718-1970-0258249-6.

39. Shanno, D.F. Conditioning of quasi-Newton methods for function minimization. *Mathematics of Computation* **1970**, *24*, 647–656. https://doi.org/10.1090/s0025-5718-1970-0274029-x.